FIBER-MATRIX ADHESION IN CFRC GREENBODIES AND ITS INFLUENCE ON MICROCRACK FORMATION DURING THE CARBONIZATION PROCESS

S.J.A. Haug, W.M. Mueller, M.G.R. Sause, S. Horn
University of Augsburg, Institute of Physics, Experimental Physics II, D-86135 Augsburg, Germany

ABSTRACT

Two types of unidirectional carbon fiber reinforced polymer greenbodies were prepared, using carbon fibers with high and low chemical surface functionality embedded in a phenolic resin matrix. The fiber-matrix adhesion in these greenbody composites was evaluated applying cyclic single fiber push-out measurements. The development of the crack pattern during carbonization was monitored using in-situ acoustic emission measurements for both sample types. After carbonization optical- and scanning electron microscopy were applied for ex-situ complementation of the acoustic emission results.
Composites with low surface functionality fibers exhibit low adhesion between fiber and matrix in the greenbody production stage, while composites with high surface functionality fibers show an order of magnitude higher adhesion prior to pyrolysis. During carbonization composites with low surface functionality fibers show an order of magnitude higher rate of crack formation than composites with high surface functionality fibers, as shown by acoustic emission activity. Based on acoustic emission analysis composites with low surface functionality fibers display a higher share of fiber-matrix debonding and subsequent interfacial crack propagation, while composites with high surface functionality fibers predominantly show matrix cracking. This fact is confirmed by electron and optical microscopy.

INTRODUCTION

The polymer infiltration and pyrolysis (PIP) production route is a common and cost efficient production process for the manufacturing of carbon fiber reinforced carbon materials (CFRC). In this process, carbon fiber reinforced polymer composites (CFRP) are used as greenbodies that are carbonized at temperatures up to 1000 °C in inert atmosphere. During the heating procedure the polymer matrix is decomposed to form amorphous carbon. In CFRP production, surface treatments like electrochemical oxidation are widespread methods to enhance the fiber-matrix adhesion[1, 2, 3]. However, it has been shown that such fiber surface treatments may lead to brittle failure and poor mechanical properties in CFRC composites manufactured via the PIP process[4, 5, 6].
In the present study, we investigate the influence of two fiber surface treatments on the PIP-process, in particular on the fiber-matrix adhesion prior to carbonization, its impact on crack growth during carbonization and on the evolving microstructure. Thus unidirectional minicomposites with two differently surface treated fibers were produced and investigated prior to-, in-situ during- and post carbonization.

SAMPLE PREPARATION

Carbon fibers

Two different types of carbon fiber surface treatment were applied to the same commercially available high tenacity fibers (Sigrafil® Epy, SGL Carbon group). The different surface treatments result in different chemical surface functionalities, which were described in more detail previously[7]. The fiber type showing high surface functionality is referred to as HF-fiber below, while the type showing low functionality is referred to as LF-fiber. Both fiber types were sized with a standard epoxy sizing.

Minicomposites

Minicomposites were prepared by manual impregnation of 50k fiber tows with standard phenolic resin. Curing took place at 170 °C and 20 bar for 25 min. Carbonization of the minicomposites was performed under N_2-atmosphere. The maximum carbonization temperature was 900 °C, the applied temperature profile is depicted in Figure 1.

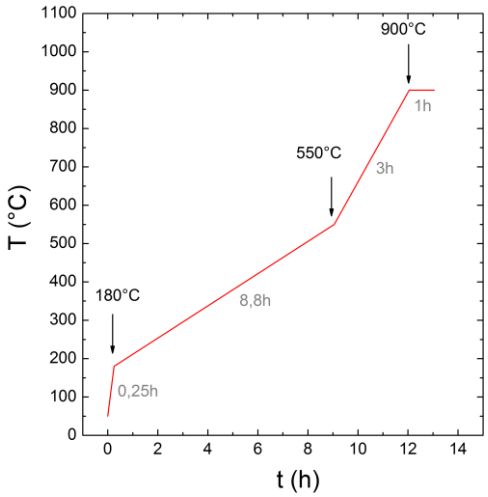

Figure 1. Temperature profile applied for composite carbonization.

Preparation of push-out samples

Before thinning the samples to the required thickness for single-fiber push-out experiments, the greenbody minicomposites were embedded in epoxy resin (Epofix, Struers GmbH) for mechanical handling issues. The embedded minicomposites were grinded and polished on one side with a standard polishing machine (Tegraforce, Struers GmbH). Subsequently, a slice of approximately 500 µm thickness was cut off from the polished sample side with a low speed diamond saw (Isomet, Buehler GmbH). In the final preparation step, the unpolished side of the sample was lapped plane-parallel to the polished side with a lapping machine (PM5, Logitech Ltd.). Sample thickness was adjusted to specific values between 35 µm and 60 µm. The thinned samples were fixed on a glass substrate across a groove with approximately 60 µm width by quartz wax.

EXPERIMENTAL METHODS

Evaluation of fiber-matrix adhesion with single fiber push-out experiments

As described in previous work[7], the greenbody samples with LF- and HF-fibers have similar fiber volume content (65 – 70 %) and porosity (10 – 15 %). To characterize the fiber-matrix-interaction of the samples on a micromechanical scale, single fiber push-out investigations were performed. To this end, a nano-indentation system (Universal Nanomechanical Tester, Asmec GmbH), featuring a positioning accuracy of 1 µm in lateral direction, was used. Experiments were conducted under displacement-controlled conditions with resolutions of 1 nm and 0.01 mN, respectively. In the present study, push-out experiments were conducted with a flat-end-cone indenter tip 5.3 µm in diameter (Figure 2). Loading rates were set to 50 nm/s. Cyclic loading (Figure 3 A) was applied to analyze the respective interfacial fracture toughness $G_{II,C} = \frac{\Delta E_{crack,stable,}}{A_{crack,stable}}$, following the approach of references [8 - 14]. $\Delta E_{crack,stable}$ refers to the total energy dissipated during stable crack growth for complete debonding of the fiber-matrix interface, corresponding to the area between the envelope- and the reloading curve resulting from cyclic loading[11,12] (orange area in Figure 3 B). $A_{crack,stable}$ denotes the area of stable crack growth. Figure 4 A shows a schematic of the dependence of crack energy on indenter displacement, for negligible plastic

matrix deformation. $\Delta E_{crack,stable}$, can be determined from the last cycle, at final failure. According to references [9,10] the interfacial fracture toughness $G_{II,C}$ can be extracted from a linear regression when plotting the crack energy (normalized by the fiber circumference U_{CF}, Figure 4 B) as a function of the sample thickness for several samples of the same type, following equation 3.1.

$$\frac{\Delta E_{crack,stable}}{U_{CF}} = G_{II,C}\,(d - l_{unstable}) \qquad (1)$$

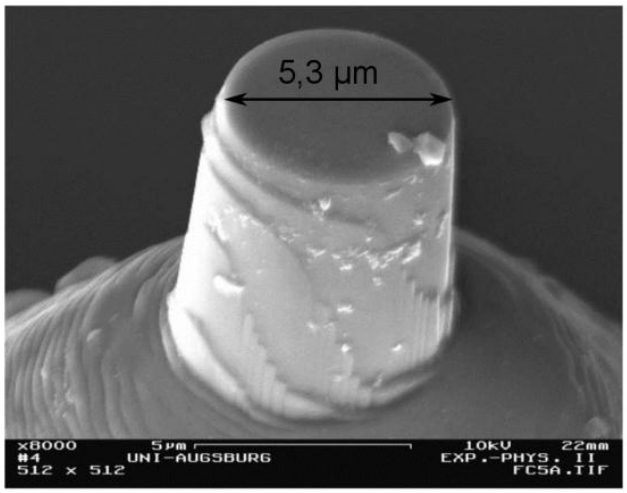

Figure 2. SEM image of the used flat-end-cone indenter tip.

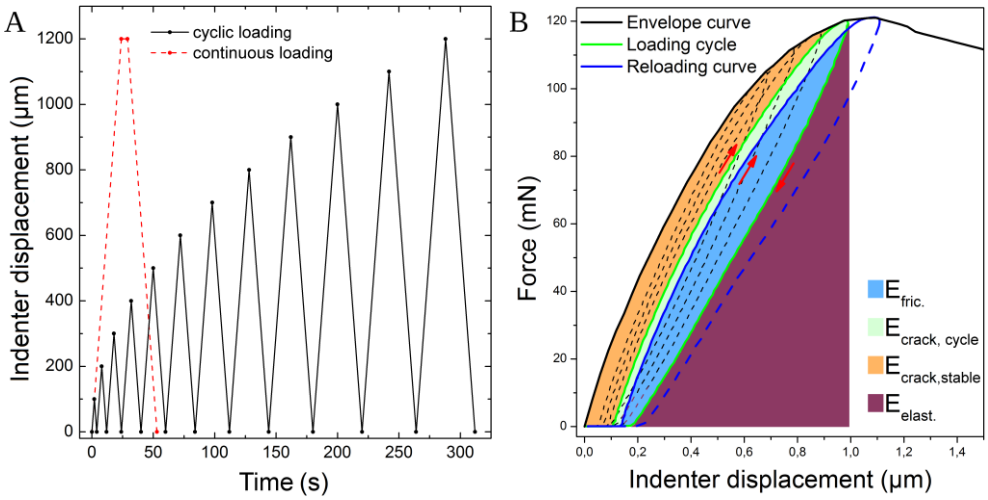

Figure 3. Cyclic loading push-out experiment, comparison of continuous and cyclic loading schedule (A), evaluation of force-displacement curve resulting from cyclic loading (B).

Here d denotes the sample thickness, while $l_{unstable}$ is the length of unstable crack growth. The York-method[15, 16] for linear fitting with X- and Y-errors was used for determination of interfacial fracture toughness, unstable crack length and their respective errors.

In-situ analysis of crack formation during carbonization with acoustic emission analysis

Acoustic emission (AE) analysis is used extensively for investigation of crack formation in CFRP[17,18,19] and ceramic matrix composites (CMC)[20,21,22] during external loading. Given the ability to detect AE online, it can also be applied to monitor crack formation processes during the carbonization step of the PIP production route[23, 24, 25, 26]. Therefore, in-situ AE-analysis was carried out in the present study during carbonization, to quantify the crack formation in CFRC. Signal recording was carried out with an USB AE-Node (USB AE Node 1283, Mistras Group, Inc.), a 26 dB preamplifier and a multiresonant

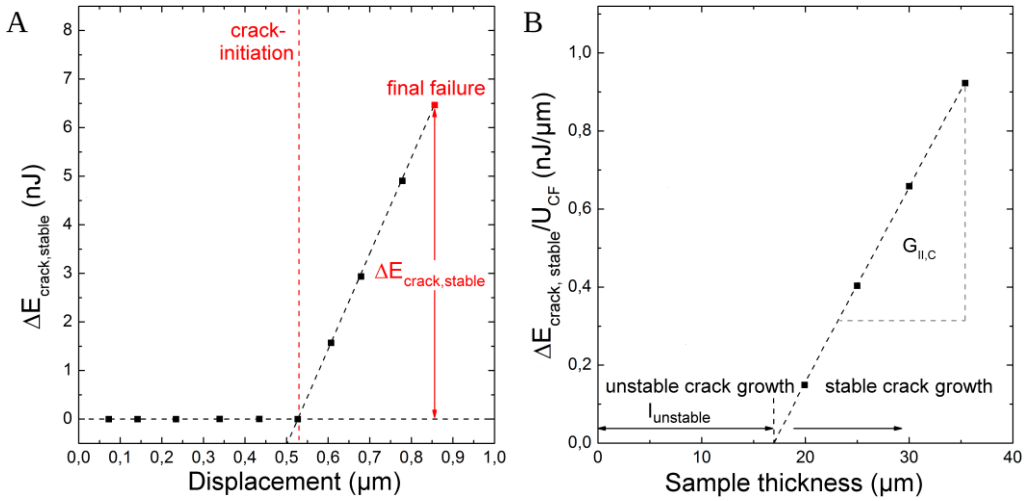

Figure 4. Interpretation of cyclic loading push-out experiments using progression of crack energy with increasing indenter displacement (A), G_{IIC} can be extracted from the linear slope of crack energy as a function of sample thickness (B).

piezoelectric sensor (WD, Mistras Group, Inc.). Based on the calculations of reference [27], a cylindrical alumina waveguide was chosen, with 5 mm diameter and 555 mm length, to guide the emitted AE signals to the outside of the oven protecting the sensor and other equipment from the high temperatures during pyrolysis. The waveguide was acoustically decoupled from the carbonization oven by a teflon shell. For both types of minicomposites, five samples of 5 mm length were prepared using a wire saw. These samples were fixed to the waveguide by an alumina glue (Fire-Cem-Adhesive type FCA1500, Firetek Norderstedt) that is temperature resistant up to 1500 °C. To investigate the noise level and influence of the adhesive, the acoustic emission of the setup was measured replacing the samples by a quadratic alumina plate of 5 mm length and 1 mm thickness. Signal classification was carried out applying a multi-feature pattern recognition approach, described in detail in reference [28]. In accordance to reference [28] the plot of the partial power 2 (equation 2) as a function of the weighted peak frequency $f_{weightedPF}$ (equation 3) was chosen to illustrate the results of the pattern recognition process.

$$\text{partial power 2} = \frac{\int_{f_1}^{f_2} U^2(f)\,df}{\int_{f_{start}}^{f_{end}} U^2(f)\,df} \quad \text{(with } f_1 = 150 \text{ kHz and } f_2 = 300 \text{ kHz)} \tag{2}$$

$$f_{weightedPF} = \sqrt{f_{peak}\, f_{centroid}} \tag{3}$$

U(f) denotes the fourier transform of the signal voltage, f_{peak} the frequency of peak signal contribution and $f_{centroid}$ the centroid of the signal fourier transform.
After the carbonization, polished cross sections of the fully carbonized CFRC samples were prepared, in order to complement the results of the AE-analysis by ex-situ optical microscopy and SEM investigations.

RESULTS

Fiber-matrix adhesion in greenbody samples

First we describe push-out experiments on samples of both types at same thickness (d = 60 µm). Figure 5 shows representative cyclic push-out curves for each, the HF- and the LF-sample. It can be seen that significantly higher forces as well as higher displacements are reached at final failure in case of the HF-sample. Figure 6 A shows the progression of crack energy, averaged over twelve cyclic push-out measurements, performed on the same sample.

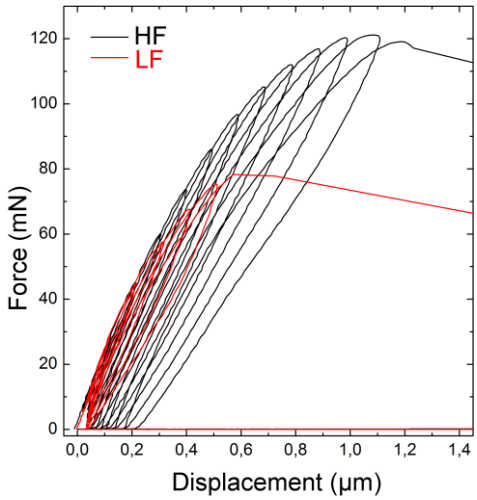

Figure 5. Comparison of push-out investigation for samples of the same thickness (d = 60 µm) using exemplary force displacement curves for both sample types.

The total crack energy for the HF-sample from crack initiation to final failure turns out to be more than 10 times the value of the LF-sample. From the individual curves, the total crack energy of stable crack growth was extracted. Figure 6 B shows the total crack energy, normalized by the mean fiber circumference, plotted as a function of the sample thickness, for both sample types. Table I shows the calculated interfacial fracture toughness as well as the unstable crack length for both sample types respectively. The interfacial fracture toughness and, consequently, the adhesion between fiber and matrix is enhanced by more than an order of magnitude when comparing HF- and LF-samples. Furthermore, the unstable crack length is reduced to approximately one third compared to LF-samples. The enhanced adhesion of the HF-fibers is attributed to the higher chemical surface functionality of the carbon fiber surface.

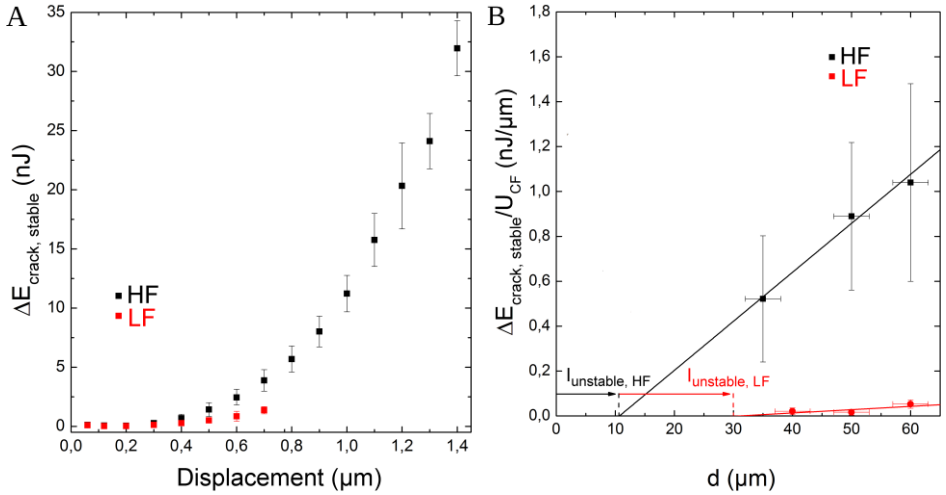

Figure 6. Extracted crack energy for both sample types, averaged values of 12 measurements (A), normalized total crack energy as a function of sample thickness (B).

Table I: Interfacial fracture toughness and unstable crack growth for both sample types

Surface treatment	$G_{II,C}$ (J/m²)	$l_{unstable}$ (µm)
HF	21.8 ± 15.7	11 ± 9
LF	1.5 ± 1.2	30 ± 26

In-situ observation and quantification of crack formation during carbonization

In our AE analysis, first the accumulated number of signals (hits) during the carbonization is depicted in Figure 7 A together with the temperature profile (blue line). For the assessment of the background noise of the setup and possible signals due to crack formation inside the adhesive layer, the alumina reference baseline-measurement was repeated three times (green lines). During heating to the set temperature of 900°C and the one-hour dwell time ($t < 13$ h), approximately 10 to 12 AE hits are detected, which can be considered negligible in comparison to the AE activity of the composite samples. During the free cooling of the oven ($t \geq 13$ h), up to 2000 hits can be detected. A similar increase in signal detection can be observed for the composite samples. Since the cooling in this regime is uncontrolled, we assume high cooling rates and hence high thermal stress in the adhesive layer in this time domain. We conclude that this sudden thermal stress leads to cracking of the adhesive layer. Consequently, only signals emitted during heating, which can clearly be assigned to the composite samples, will be considered in the following. At 13 h carbonization time (29680 ± 1266) hits are accumulated, averaged over the five LF- samples measured, while only (1940 ± 649) hits are accumulated for HF-samples.

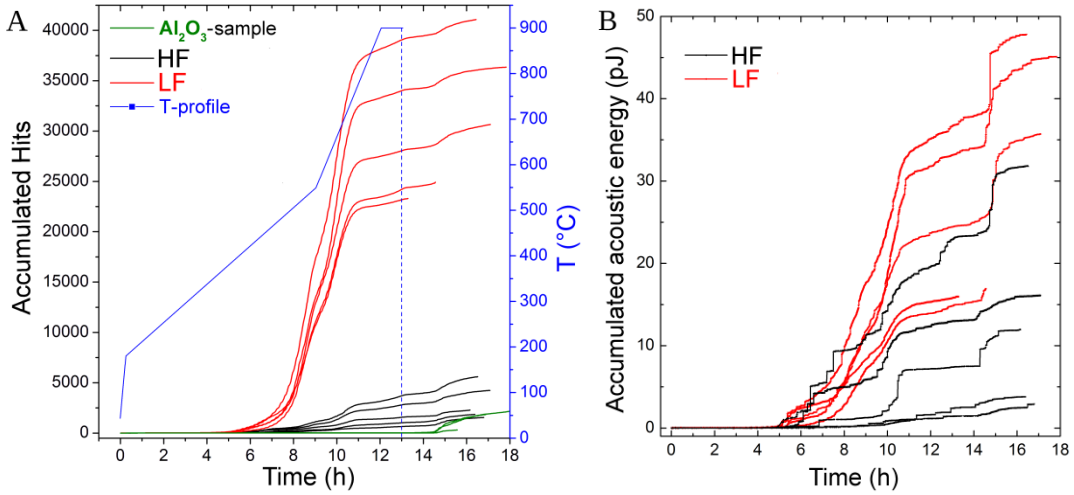

Figure 7. In-situ AE-analysis of crack formation during carbonization, accumulated number of signals (hits) of Al_2O_3 reference and composite samples (A), accumulated acoustic energy of composite sample (B).

Assuming that every signal corresponds to an individual crack event, the rate of crack formation of LF-samples is one order of magnitude higher than that of HF-samples. The onset of the acoustic activity can be correlated to the onset of volume- and mass shrinkage at 360 °C (4.5 h), as determined by thermo-physical investigations, tightly linking the occurrence of cracks to the volumetric shrinkage of the matrix.
Furthermore, the accumulated acoustic energy (Figure 7 B) is evaluated. For LF-samples the accumulated acoustic energy after 13 h amounts to (24.9 ± 9.8) pJ, while (9.4 ± 8.8) pJ are detected for HF-samples. Because of the proportionality of acoustic energy to micromechanically released strain energy[17] a higher level of damage is expected for LF-samples. Since the number of signals is one order of magnitude higher for LF-samples, but only a threefold increase in acoustic energy can be detected, it can be deduced that the amount of micromechanical damage per crack event is higher for HF-samples. This is also suggested by the pronounced steps in accumulated energy curves of HF-samples (Figure 7 B), indicating single AE signals with high energy release and therefore high micromechanical damage. In contrast, a smooth progression of the energy curve is observed for LF-samples, with only small amounts of energy per signal.

Signal classification

For both sample types the pattern recognition algorithm proposes separation into two clusters. Figure 8 A and B show the results of the pattern recognition process for both sample types projected to the partial power 2 weighted peak frequency plane. In this plot the AE signals of the five samples investigated where combined to provide a better overview of the general material behavior. The clusters of both sample types lie in the same spectral range, indicating that the same fracture mechanisms are present. Absolute signal count and relative signal distribution, however, differ. Figure 9 depicts the relative share of signal classes for both sample types. It can be observed, that the relative share of high frequency signals is higher for LF-samples compared to HF-samples.

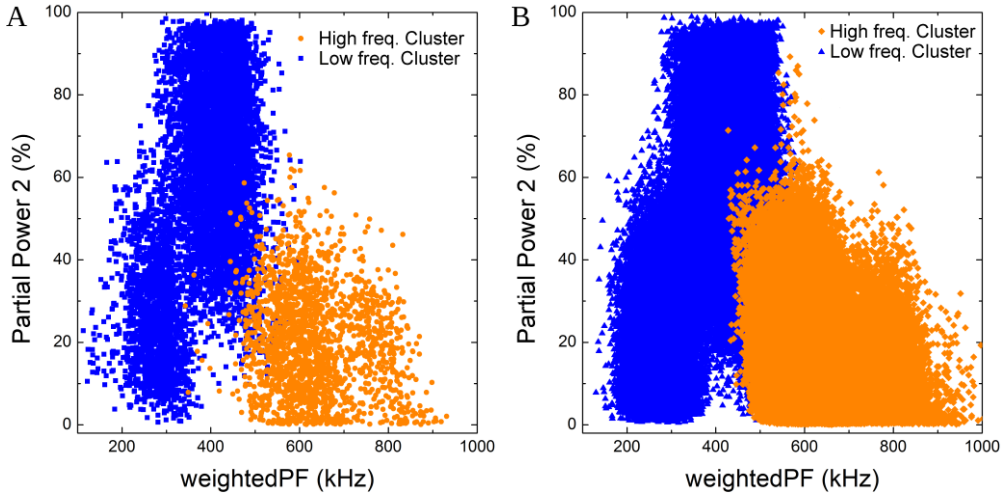

Figure 8. Partial Power 2 over weighted peak frequency, HF-samples (A), LF-samples (B). Pattern recognition algorithm proposes two clusters (orange and blue coloring).

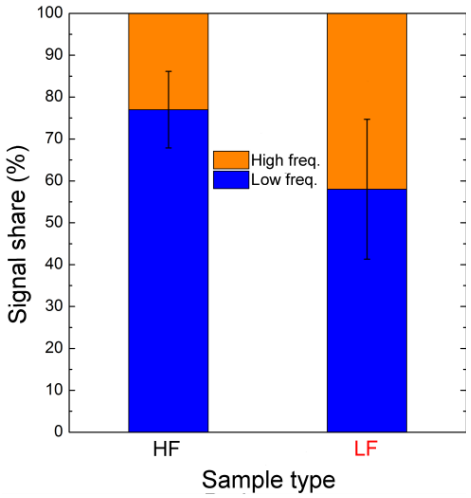

Figure 9. Relative share of signal types for both sample types as distinguished by pattern recognition.

Ex-situ investigation of the crack pattern of carbonized samples

To further investigate the source of the AE signals, polished cross sections were prepared from the samples used in the in-situ AE study. Cross sections were examined by optical microscopy and electron microscopy. Figures 10 A and B show a SEM micrograph of a matrix crack of characteristic dimension, determined by the characteristic size of matrix regions in these samples and an inter-fiber crack for the HF-sample. Both types of cracks occur on both sample types. It can be seen that the observed matrix cracks start and end propagation at the fiber-matrix interface. We suggest the following model for crack initiation

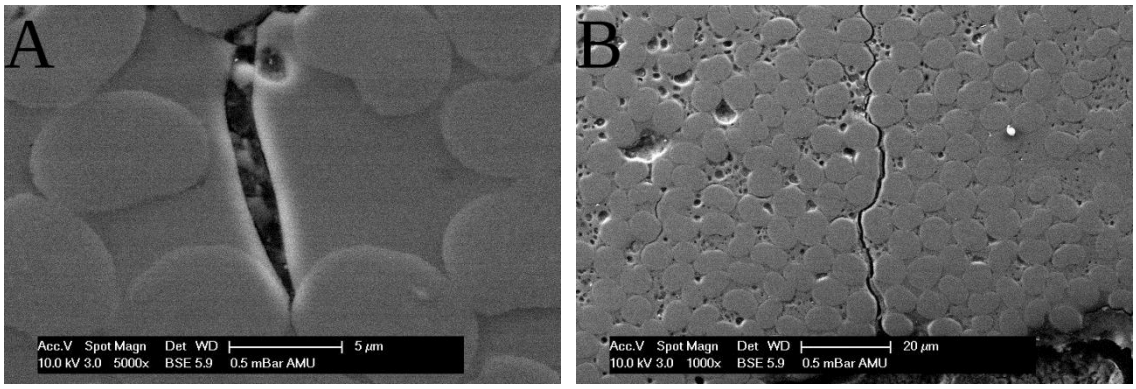

Figure 11. SEM image of characteristic crack structures, crack through a matrix cluster of characteristic dimension (A), inter-fiber crack bridging across multiple adjacent fibers (B)

and propagation during carbonization: cracks are initiated at the fiber-matrix interface and propagate either along the fiber-matrix interface or through the matrix. In case of HF-samples, due to the strong fiber-matrix adhesion, crack propagation occurs dominantly through the matrix while for LF-samples crack propagation along the fiber-matrix interface is favorable due to the weak fiber-matrix adhesion. In this case crack growth occurs as a sequence of multiple subsequent debondings of adjacent fiber-matrix interfaces, detected by AE as a cracking event. For CFRP the AE-signals of cracks propagating along a fiber-matrix interface are expected to exhibit a higher frequency content than signals of cracks propagation within the matrix material[18]. This shift in frequency might be due to the higher propagation velocities of cracks propagating along an interface between two media, with respect to the medium with lower propagation velocities[29,30,31]. We therefore conclude that the high frequency signal cluster corresponds to the interfacial crack propagation while the low frequency signal cluster corresponds to matrix cracking in the present case.
To compare the relative distribution of matrix cracks and interface cracks in HF- and LF-samples, optical micrographs with lower magnification are reviewed.

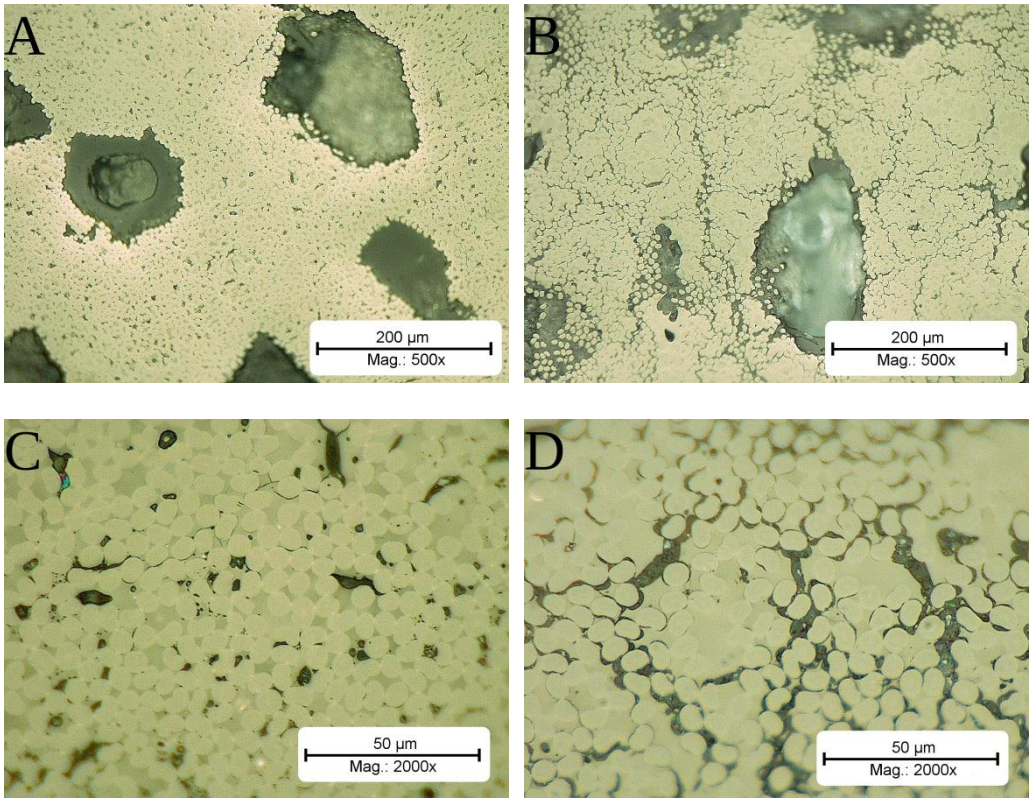

Figure 10. Optical micrographs of cross sections through carbonized samples, HF-sample; magnification 500x (A), LF-sample; magnification 500x (B), HF-sample; magnification 2000x (C), LF-sample; magnification 2000x (D).

Figures 11 A and C show optical micrographs of HF-samples in different magnifications, while Figures 11 B and D show the corresponding images for LF-samples. HF-samples show a low crack density with matrix cracks dominating. Few cracks are observed propagating along the interface between fibers and matrix. For LF-samples the higher crack density suggested by AE-analysis is clearly confirmed by microscopy. Matrix cracks are found in much higher density than for HF-samples. In contrast to the HF-samples, a high density of interfacial cracks is observed comparable to that of matrix cracks. The lower surface functionality of LF-fibers promotes fiber-matrix debonding and subsequently enhanced interfacial crack propagation compared to HF-samples during carbonization. The higher density of both types of cracks in the LF-samples can be attributed to the easier crack initiation at the fiber-matrix interface.

SUMMARY AND CONCLUSION

During the carbonization reaction the phenolic resin matrix shrinks by more than 65 vol%, while the fiber dimensions remain nearly unchanged. Therefore, high shrinkage stress arises during carbonization. The fiber-matrix adhesion in CFRP greenbodies has a strong influence on the crack structure emerging during carbonization. We were able to show that the fiber-matrix adhesion in greenbody samples is strongly influenced by the chemical surface functionality of the carbon fiber. In composites with low fiber-matrix adhesion (LF-samples) fiber-matrix debonding occurs more frequently than in composites with high fiber-matrix adhesion (HF-samples), providing sites for crack initiation. This results in a much higher crack density for LF-materials than for HF-materials and at the same time for a higher proportion of interfacial cracks. The crack pattern of HF-materials is dominated by matrix cracks. The results show clearly that by variation of the fiber-matrix interaction in CFRP greenbodies the crack structure in CFRC materials can be controlled.

REFERENCES

[1] L. T. Drzal, M. J. Rich, P. F. Lloyd: Adhesion of Graphite Fibers to Epoxy Matrices: I. The Role of Fiber Surface Treatment, *The Journal of Adhesion*, 16, 1, 1983, pp. 1–30.

[2] K. Tsutsumi, S. Ishidal, K. Shibata: Determination of the surface free energy of modifiedcarbon fibers and its relation to the work of adhesion, *Colloid Polym Sci*, 268, 1, 1990, pp31-37.

[3] L. Tang, J. L. Kardos: A Review of methods for improving the interfacial adhesion between carbon fiber and polymer matrix, *polymer composites*, 18, 1, 1997, pp. 100-113.

[4] L. M. Manocha, E.Yasuda, Y. Tanabe: Effect of carbon fiber surface-treatment on mechanical properties of C/C composites, *Carbon*, 26, 3, 1988, 333-337

[5] L. M. Manocha, O. P. Bahl, Y. K. Singh: Mechanical behaviour of carbon-carbon composites made with surface treated carbon fibers, *Carbon*, 27, 3, 1989, 381-387

[6] E. Fitzer, K.-H. Geigl, W.Hüttner: The influence of carbon fiber surface treatment on the mechanical properties of carbon/carbon composites, *Carbon*, 18, 4, 1980, 265-270

[7] S. J. A. Haug, W. M. Mueller, S. Horn: influence of carbon-fiber surface treatment on the properties of CFRC mateials, *Proceedings of the 20th international conference on composite materials*, Copenhagen, 2015

[8] W.M. Mueller, J. Moosburger-Will, M.G.R. Sause, S. Horn: Microscopic analysis of single-fiber push-out tests on ceramic matrix composites performed with Berkovich and flat-end indenter and evaluation of interfacial fracture toughness*, Journal of the European Ceramic Society*, 33, 2, 2013, pp. 441-451.

[9] W.M. Mueller, J. Moosburger-Will, M. Greisel, S. Horn: Quantification of the crack areas in ceramic matrix composites at single-fiber push-out testing and influence of pyrocarbon

fiber coating thickness on interfacial fracture toughness, *Journal of the European Ceramic Society*, 35, 11, 2015, pp. 2981-2989.
[10] W.M. Mueller, J. Moosburger-Will, M. Greisel, S. Horn: Quantification of the crack areas of stable and unstable crack propagation during single-fiber push-out tests performed on ceramic matrix composite samples, *Proceedings of the 20th international conference on composite materials*, Copenhagen, 2015
[11] J. Jäger, M.G.R. Sause , F. Burkert, J. Moosburger-Will, M. Greisel, S. Horn: Influence of plastic deformation on single-fiber push-out tests of carbon fiber reinforced epoxy resin, *Composites Part A: Applied Science and Manufacturing*, 71, 2015, pp. 157-167
[12] M. Greisel , J. Jäger, J. Moosburger-Will, M.G.R. Sause, W.M. Mueller, S. Horn: Influence of residual thermal stress in carbon fiber-reinforced thermoplastic composites on interfacial fracture toughness evaluated by cyclic single-fiber push-out tests, *Composites Part A: Applied Science and Manufacturing*, 66, 2014, pp. 117-127.
[13] M. Greisel, M. Schulz, W.M. Mueller, J. Moosburger-Will, S. Horn: Evaluation of the Interfacial fracture toughness of a carbon fiber reinforced thermoplastic composite by cyclic single fiber push-out tests, *Proceedings of the 20th international conference on composite materials*, Copenhagen, 2015
[14] A. Battisti , D. Esqué-de los Ojos , R. Ghisleni , A. J. Brunner: Single fiber push-out characterization of interfacial properties of hierarchical CNT-carbon fiber composites prepared by electrophoretic deposition, *Composites Science and Technology*, 95, 2014, pp. 121-127
[15] D. York : Least-squares fitting of a straight line, *Canadian Journal of Physics*, 44, 5, 1966, 1079-1086
[16] D. York, N. M. Evensen, M. L. Martinez, J. D. Delgado: Unified equations for the slope, intercept, and standard errors of the best straight line, *American Journal of Physics*, 72, 3.
[17] M. G. R. Sause, F . Haider, S. Horn: Quantification of metallic coating failure on carbon fiber reinforced plastics using acoustic emission, *Surface and Coatings Technology*, 204, 3, 2009, 300-308
[18] M. G. R. Sause, S. Horn: Simulation of acoustic emission in planar carbon fiber reinforced plastic specimens, *Journal of Nondestructive Evaluation*, 29, 2, 2010, 123-142
[19] M. G. R. Sause, S. Richler: Finite Element Modelling of Cracks as Acoustic Emission Sources, *Journal of Nondestructive Evaluation*, 34,1, 2015, 1-13
[20] G.N. Morscher, J. Martinez-Fernandez, M. J. Purdy: Determination of Interfacial Properties Using a Single-Fiber Microcomposite Test, *Journal of the American Ceramic Society*, 79, 4, 1996, 1083-1091
[21] G. N. Morscher, A. L. Gyekenyesi: The velocity and attenuation of acoustic emission waves in SiC/SiC composites loaded in tension, *Composites Science and Technology*, 62, 9, 2002, 1171-1180
[22] G. N. Morscher, H. Yun, J. A. DiCarlo: In-Plane Cracking Behavior and Ultimate Strength for 2D Woven and Braided Melt-Infiltrated SiC/SiC Composites Tensile Loaded in Off-Axis Fiber Directions, Journal of the American Ceramic Society, 90, 10, 2007, 3185-3193
[23] J. R. Bulau: AE monitoring for control of carbon-carbon pyrolysis, *Proceedings of the IEEE Ultrasonics Symposium* , 1988, 1057-1063
[24] B. R Tittmann, C.E. Yen: Acoustic emission technique for monitoring the pyrolysis of composites for process control , Ultrasonics, 48, 6, 2008, 621-630
[25] B. R Tittmann: Acoustical studies of damage mechanisms in carbon-carbon during first carbonization, *Proceedings of the IEEE Ultrasonics Symposium* , 1989, 627-630
[26] J. Schulte-Fischedick, M.Frieß, W.Krenkel. R. Kochendörfer: Crack microstructure during the carbonization of carbon fiber reinforced plastics to carbon/carbon compsites, *Proceedings of 12th International Conference on Composite Materials*, 1999
[27] A. Zelenyak, M. Hamstad, M. G. R. Sause: Modeling of Acoustic Emission Signal Propagation in Waveguides, *Sensors*, 15, *5*, 2015, 11805-11822

[28] M. G. R. Sause, A. Gribov, A. R, Unwin, S. Horn: Pattern recognition approach to identify natural clusters of acoustic emission signals, *Pattern Recognition Letters*, 33, 1, 2012, 17-23
[29]C. Liu, J. Lambros, A. J Rosakis: Highly transient elastodynamic crack growth in a bimaterial interface: higher order asymptotic analysis and optical experiments, *Journal of the Mechanics and Physics of Solids*, 41,12, 1993, 1887-1954
[30]J. Lambros, A. J. Rosakis: Shear dominated transonic interfacial crack growth in a bimaterial-I. Experimental observations, *Journal of the Mechanics and Physics of Solids*, 43, 2, 1995, 169-188
[31]C.Liu, Y. Huang, A.J. Rosakis: Shear dominated transonic interfacial crack growth in a bimaterial I-II. Asymptotic fields and favorable velocity regimes, *Journal of the Mechanics and Physics of Solids*, 43, 2, 1995, 189-206